An Integrated TKE-Based Eddy Diffusivity/Mass Flux Boundary Layer Closure for the Dry Convective Boundary Layer

MARCIN L. WITEK, JOAO TEIXEIRA, AND GEORGIOS MATHEOU

Jet Propulsion Laboratory, California Institute of Technology, Pasadena, California

(Manuscript received 7 May 2010, in final form 17 November 2010)

ABSTRACT

This study presents a new approach to the eddy diffusivity/mass flux (EDMF) framework for the modeling of convective boundary layers. At the root of EDMF lies a decomposition of turbulent transport mechanisms into strong ascending updrafts and smaller-scale turbulent motions. The turbulent fluxes can be therefore described using two conventional approaches: mass flux (MF) for the organized thermals and eddy diffusivity (ED) for the remaining turbulent field. Since the intensities of both MF and ED transports depend on the kinetic energy of the turbulent motions, it seems reasonable to formulate an EDMF framework based on turbulent kinetic energy (TKE). Such an approach allows for more physical and less arbitrary formulations of parameters in the model. In this study the EDMF–TKE coupling is achieved through the use of (i) a new parameterization for the lateral entrainment coefficient ε and (ii) the MF contribution to the buoyancy source of TKE. Some other important features of the EDMF parameterization presented here include a revised mixing length formulation and Monin–Obukhov stability scaling for the surface layer. The scheme is implemented in a one-dimensional (1D) model. Several cases of dry convective boundary layers (CBL) with different surface sensible heat fluxes in the free-convection limit are investigated. Results are compared to large-eddy simulation (LES). Good agreement between LES and the 1D model is achieved with respect to mean profiles, boundary layer evolution, and updraft characteristics. Some disagreements between the models are found to most likely relate to deficiencies in the TKE simulation in the 1D model. Comparison with other previously established ε parameterizations shows that the new TKE-based formulation leads to equally accurate, and in many respects better, simulation of the CBL. The encouraging results obtained with the proposed EDMF framework indicate that full integration of EDMF with higher-order closures is possible and can further improve boundary layer simulations.

1. Introduction

Turbulent transport in the boundary layer (BL) controls the exchange of heat, moisture, and pollutants between the surface and the free troposphere. The importance of turbulent mixing to the BL structure and evolution is well recognized (Wyngaard 1992). The stochastic nature of turbulence and the various scales of motions involved, however, make the problem particularly difficult to address analytically or numerically. The eddy diffusivity (ED) method used to represent vertical turbulent fluxes has been fairly successful in a number of atmospheric conditions. Also referred to as a small-eddy closure, ED has important physical limitations related to its locality (e.g., Stull 1988). It transports quantities locally down their mean gradient and fails to represent upward fluxes in situations where there are well mixed (zero gradient) or slightly stable average profiles. Such conditions are commonly observed in the convective boundary layer (CBL) where a large part of turbulent transport is carried out by strong thermals or convective plumes (Schumann and Moeng 1991a; Randall et al. 1992; Moeng and Sullivan 1994; Cheinet 2003). Attempts to take these nonlocal transport effects into account have been twofold: by extending an ED approach with a nonlocal countergradient term (Deardorff 1966; Holtslag and Moeng 1991; Stevens 2000) or using solely a mass flux (MF) scheme instead of ED (Wang and Albrecht 1990; Randall et al. 1992; Lappen and Randall 2001; Cheinet 2003). The bulk MF approach has been mainly used for the parameterization of shallow and deep moist convection (e.g., Ooyama 1971; Betts 1973; Arakawa and Schubert 1974). Lately both ED and MF

Corresponding author address: Marcin L. Witek, Jet Propulsion Laboratory, California Institute of Technology, 4800 Oak Grove Drive, Pasadena, CA 91109.
E-mail: marcin.l.witek@jpl.nasa.gov

DOI: 10.1175/2011JAS3548.1

approaches have been combined to address local and nonlocal turbulent transport in a single eddy diffusivity/mass flux (EDMF) parameterization.

The EDMF framework has been in use in boundary layer modeling for almost a decade. It was introduced by Siebesma and Teixeira (2000) and since then many authors have successfully incorporated this approach to study dry and cloudy boundary layers (Soares et al. 2004; Angevine 2005; Hurley 2007; Siebesma et al. 2007; Soares et al. 2007; Neggers et al. 2009; Neggers 2009). A detailed description of the scheme along with a conceptual evaluation can be found in Siebesma et al. (2007). In short, turbulence in the convective boundary layer is conceptually divided into strong thermals and the remaining turbulent field consisting of smaller-sized eddies. Accordingly, vertical turbulent fluxes of a conserved scalar variable ϕ are decomposed into two terms (Siebesma et al. 2007):

$$\overline{w'\phi'} \cong \overline{w'\phi'}^{e} + M(\phi_u - \overline{\phi}), \tag{1}$$

where the first term on the right-hand side represents turbulent transport by small-size eddies and the second transport term is associated with strong updrafts. The first term is often denoted environmental flux (hence the subscript e) and is parameterized with an ED approach, whereas the other is the mass flux transport. In Eq. (1) $M = \sigma w_u$ in which w_u is the updraft velocity, ϕ_u is the scalar value in the updrafts, and σ the area fraction occupied by updrafts. An important approximation embedded in Eq. (1) is that $\sigma \ll 1$ and $\phi^e \cong \overline{\phi}$. In previous EDMF formulations the area fraction σ is fixed, usually chosen to be 0.1 (Soares et al. 2004; Neggers et al. 2009) or a similar value (Siebesma et al. 2007; Soares et al. 2007). Variable σ is often assumed in MF closures of shallow cumulus or well-mixed layers (e.g., Arakawa and Schubert 1974; Randall et al. 1992; Lappen and Randall 2001), where there is no ED transport included. Such approach could be also employed in EDMF, as was partially demonstrated by Neggers et al. (2009) who used two updrafts (dry and wet) for shallow moist convection with a variable area fraction between them. Setting σ to a constant value reduces the problem of determining mass flux M to finding the w_u profile. The area fraction represents the percentage of the w_u distribution (regardless of the distribution's width and skewness) that is associated with the MF component.

Most of the EDMF schemes developed so far use various combinations of first-order and 1.5-order closure BL parameterizations (Stull 1988). Siebesma et al. (2007) use a prescribed ED coefficient profile and a prescribed vertical velocity variance profile to close the EDMF parameterization. Neggers et al. (2009) use a prescribed ED profile method and a diagnostic equation for the updraft vertical velocity (Simpson and Wiggert 1969). Soares et al. (2004) and Angevine (2005) parameterize the ED coefficient based on a turbulent kinetic energy (TKE) closure. An original extension of the TKE-based scheme is proposed by Soares et al. (2007). They parameterize the MF term based on the vertical velocity variance, which is assumed to be a simple function of TKE. Since in their scheme the MF term is directly related to TKE, derivation of w_u is no longer necessary to close the parameterization. A recent development of the EDMF framework was presented by Angevine et al. (2010). Some novel aspects of their work include using the total turbulent energy to close the parameterizations and applying the EDMF approach to the total turbulent energy vertical transport term.

An important parameter of the EDMF scheme—the lateral entrainment coefficient ε that controls the exchanges between the updrafts and the environment and hence the updraft evolution—is typically parameterized based on two approaches. Authors use either a prescribed ε profile depending on the inversion height or a function proportional to the inverse of the updraft velocity.

In this study we introduce a fully coupled EDMF scheme based on a TKE closure. To allow for a closer EDMF–TKE integration we propose a new lateral entrainment parameterization based on TKE. Through the use of this new approach, TKE is linked to both the ED transport and MF transport mechanisms. The feedback of EDMF to TKE is realized through the buoyancy source term in the TKE prognostic equation. The proposed EDMF scheme also includes a surface stability scaling based on the Monin–Obukhov (1954) similarity theory that allows for more realistic representation of the surface layer. The scheme is implemented in a 1D model and validated against large-eddy simulation (LES) results for a variety of different conditions. As a testing framework we use variants of the well-established Nieuwstadt et al. (1992) dry convective boundary layer case.

In section 2 the details of the EDMF parameterizations used in the 1D model are described. Different lateral entrainment parameterizations that are used for intercomparison studies are also reviewed. Section 3 introduces the LES setup and simulation results for the dry CBL cases investigated in the present study. Results of 1D simulations and comparison with LES are presented in section 4. In section 5 different ε formulations and their influence on the 1D simulations are studied. Finally, conclusions and closing remarks are presented in section 6.

2. One-dimensional model

The one-dimensional model used in this study is a vertical transport model based on the TKE prognostic equation (e.g., Stull 1988). Full coupling with the TKE

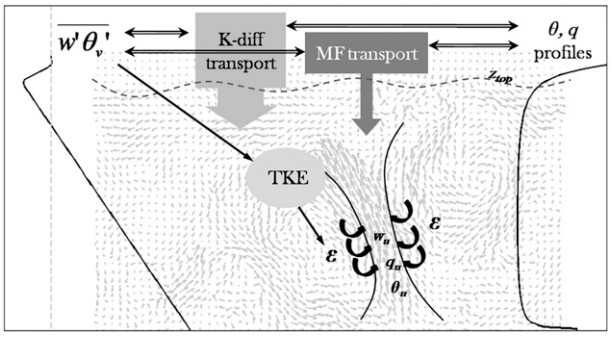

FIG. 1. Schematic of the new approach showing coupling between TKE and EDMF, embedded in a sample velocity field cross section from a LES simulation of a dry CBL. Symbols are described in the text.

allows for a more physical formulation of the turbulent mixing process as well as a less arbitrary specification of other key parameters of the model. A general schematic of the approach is presented in Fig. 1, which also shows a cross section of the velocity field from a LES simulation of a dry CBL. The scheme distinguishes two turbulent transport mechanisms: mass flux and eddy diffusivity. Both processes affect the θ and q profiles as well as the buoyancy source term of the TKE prognostic equation. TKE influences mass exchange between the updrafts and environment (via the ε coefficient, described later in the text) and therefore the updraft properties and evolution. The updrafts, in turn, affect the MF transport and buoyancy, which closes the coupling cycle between TKE and EDMF. The important impact of TKE in the lateral entrainment coefficient is a good reminder that the TKE represents not only small-scale mixing but also a significant part of the large-scale transport. All features of the new 1D model are described below.

a. General equations

The prognostic equation for a scalar $\phi \in (\theta, q)$ can be written as

$$\frac{\partial \overline{\phi}}{\partial t} = -\frac{\partial \overline{w'\phi'}}{\partial z} + F_\phi, \tag{2}$$

where w is the vertical velocity and F_ϕ is a source term. The prime denotes perturbations from the horizontal mean. In this study we investigate the free convection limit without any large-scale wind components. We therefore neglect prognostic equations for horizontal wind components and simplify the TKE prognostic equation. Vertical turbulent fluxes are parameterized in terms of the EDMF approach (Siebesma and Teixeira 2000; Siebesma et al. 2007)

$$\overline{w'\phi'} \cong -K_\phi \frac{\partial \overline{\phi}}{\partial z} + M(\phi_u - \overline{\phi}), \tag{3}$$

where K_ϕ is the ED coefficient for a variable ϕ, ϕ_u is the updraft value of ϕ; and $M = \sigma w_u$ is the mass flux divided by air density, σ representing the area fraction of updrafts, and w_u the updraft vertical velocity. Here we assume a fixed updraft fraction $\sigma = 0.1$ (Soares et al. 2004; Neggers et al. 2009). The MF closure therefore relies mainly on an accurate derivation of updraft properties w_u and ϕ_u.

After simplifications, the TKE prognostic equation takes the form (e.g., Stull 1988)

$$\frac{\partial e}{\partial t} = -\frac{\partial}{\partial z}\left(-K_e \frac{\partial e}{\partial z}\right) + \frac{g}{\overline{\theta}_v}\overline{w'\theta_v'} - D, \tag{4}$$

where e is TKE, K_e is the ED coefficient of e, g is the acceleration of gravity, $\overline{\theta}_v = \overline{\theta}(1 + 0.61\overline{q})$ is the virtual potential temperature, $\overline{w'\theta_v'}$ is the buoyancy flux, and D is the dissipation term. Note that the $\overline{w'\theta_v'}$ term in the TKE equation is parameterized using Eq. (3). This assures a proper buoyancy profile, which is strongly influenced by the MF term, especially in the slightly stable parts of the BL and at the inversion (Soares et al. 2007).

b. Parameterizations

To solve the prognostic Eqs. (2) and (4), additional equations and parameterizations need to be introduced. These include parameterizations of the ED coefficients (K_ϕ, K_e), the TKE dissipation term D, and diagnostic equations for ϕ_u and w_u, which describes M.

The ED coefficients are described by

$$K_{\phi,e} = C_{\phi,e} l \sqrt{e}, \tag{5}$$

where $C_\phi = 0.25$ and $C_e = 0.425$ are coefficients and l is the mixing length. Coefficients C_ϕ and C_e are different because ϕ turbulent mixing is resolved separately by ED and MF. So far there is no equivalent MF term for the TKE transport; therefore, a larger C_e coefficient is required. A more detailed discussion will be presented in the following sections.

The mixing length is a key parameter that highly influences the potential temperature profiles as well as the entrainment at the CBL inversion. In the case of CBLs the θ profile is often characterized by a highly unstable surface layer, a well-mixed interior, and a capping inversion. The surface layer profile is a consequence of the strong surface heating and the reduced diffusivity due to proximity to the fixed boundary. This profile is often not well represented in numerical models. However, in the EDMF approach, which includes nonlocal mixing, resolving the surface profile is important for obtaining realistic updraft characteristics. Updraft properties, in turn,

affect the entrainment and evolution of the boundary layer. The mixing length used here is a combination of formulations by Nakanishi (2001) for the surface layer and Teixeira and Cheinet (2004) for the well-mixed layer and is expressed as

$$\frac{1}{l} = \frac{1}{l_1} + \frac{1}{l_2}, \quad l_1 = \tau\sqrt{e}, \quad l_2 = kz(a + b\zeta)^c, \tag{6}$$

where l_1 is the mixing length adopted after Teixeira and Cheinet (2004) and Teixeira et al. (2004), whereas l_2 is the mixing length introduced by Nakanishi (2001). In l_1, τ is the characteristic eddy-turnover time scale specified by

$$\tau = 0.5 z_*/w_*. \tag{7}$$

In Eq. (7) z_* is the boundary layer height and w_* is the free-convection velocity scale [definition given below in Eq. (10)]. The coefficient 0.5 has been incorporated after Teixeira and Cheinet (2004), who also propose the possibility of using a constant τ, for example, 600 s. We found that such simplification has a negative impact on the quality of simulations. An equivalent to the l_1 mixing length formulation has also shown good results in cloudy boundary layers (Cheinet and Teixeira 2003). In l_2, k is the von Kármán constant, z is the height above the surface, $\zeta = z/L$ is the nondimensional surface stability parameter, L is the Obukhov length [Eq. (8)], and a, b, and c are empirical constants. Incorporating the stability parameter ζ in l_2 accounts for deviations from the mixing length at neutral conditions, given simply by kz (e.g., Blackadar 1962; Stull 1988). For unstable conditions the constants were determined to be $a = 1$, $b = -100$, and $c = 0.2$ (Nakanishi 2001). Recent studies by Suselj and Sood (2010) on the wind profile in the unstable surface layer confirmed the credibility of such l_2 formulation.

The stability parameter ζ is a function of the Obukhov length, defined as

$$L \equiv -\frac{u_*^3 \theta_v}{kg\overline{w'\theta_v'}^s}, \tag{8}$$

where $u_* \equiv (\overline{u'w'}^2 + \overline{v'w'}^2)^{1/4}$ is the friction velocity and $\overline{w'\theta_v'}^s$ is the surface buoyancy flux. In the limit of negligible large-scale wind velocity considered here, finding u_* is a more complicated process. For that the Monin and Obukhov (1954) similarity theory with the free-convection correction proposed by Beljaars (1995) is employed. Below we describe a procedure for finding u_* based on w_* and nondimensional stability functions. A broader overview of the method adopted here can be found in Abdella and McFarlane (1996).

In the limit of zero mean horizontal wind speed we can write, following Abdella and McFarlane,

$$u_* = \frac{k\alpha w_*}{\psi_M}, \tag{9}$$

where α is a coefficient on the order of unity, w_* is the free-convection velocity scale, and ψ_M is the stability function for momentum. In Eq. (9) w_* and ψ_M are given by

$$w_* = \left(\frac{z_* g}{T}\overline{w'\theta_v'}^s\right)^{1/3}, \tag{10}$$

$$\psi_M = \ln\left(\frac{z_1}{z_0}\right) - \varphi_M\left(\frac{z_1}{L}\right) + \varphi_M\left(\frac{z_0}{L}\right), \tag{11}$$

where $z_1 = 10$ m and $z_0 = 0.001$ m. The function φ_M is given after Paulson (1970) as

$$\varphi_M(x) = 2\ln(1 + x) + \ln(1 + x^2) - 2\arctan(x), \quad x = (1 - 16\zeta)^{1/4}. \tag{12}$$

The set of Eqs. (9)–(12) is solved iteratively to obtain u_* and L with a required accuracy. Having L allows the computation of l_2, which closes the mixing length parameterization given by Eq. (6). The values of u_* and w_* are also used in the TKE prognostic equation, allowing the derivation of the TKE equation surface boundary condition. After Potty et al. (2001) we use the following formulation for TKE at the surface:

$$e_s = 3.75u_*^2 + 0.2w_*^2. \tag{13}$$

TKE at the upper boundary is set to zero. The TKE dissipation term is parameterized by $D = c_e e^{3/2}/l_e$ with $c_e = 0.304$ and $l_e = l$. This formulation of the mixing length for dissipation l_e is different from that used by Teixeira and Cheinet (2004), which includes an additional scaling factor 1/2.5. Using this additional scaling is equivalent to changing the c_e coefficient. We found that setting c_e to 0.304 gives better agreement with LES simulations.

Finally, the updraft variables ϕ_u and w_u are determined by following Soares et al. (2004):

$$\frac{\partial \phi_u}{\partial z} = -\varepsilon(\phi_u - \overline{\phi}); \tag{14}$$

$$w_u\frac{\partial w_u}{\partial z} = -\varepsilon b_1 w_u^2 + b_2 B, \tag{15}$$

where ε is the lateral entrainment rate of the surrounding air into the updrafts, $b_1 = 1$ and $b_2 = 2$ are coefficients, and $B = g(\theta_{v,u}/\overline{\theta}_v - 1)$ represents the buoyancy source

term. The entrainment coefficient parameterizations will be discussed in more detail below. Solving the updraft equation for ϕ_u requires specification of the surface boundary condition, which is done using (Soares et al. 2004):

$$\phi_{u,s} = \overline{\phi}_s + \beta \frac{\overline{w'\phi'_s}}{\sqrt{e}}. \tag{16}$$

Here subscript s denotes the surface or close to the surface values, and $\beta = 0.3$ is a coefficient; w_u values at the surface are set to zero.

c. Entrainment coefficient formulations

Lateral entrainment of environmental air into updrafts affects the updraft evolution and dynamics. Highly entraining updrafts quickly lose their buoyancy before reaching the inversion. They transport surface layer properties into the middle of the boundary layer without a significant impact on the boundary layer growth. Weakly entraining updrafts preserve their buoyancy throughout the BL and penetrate the inversion, contributing to the mass and energy exchange at the interface, thus invigorating the BL growth. Accordingly, an adequate description of the updraft lateral entrainment is crucial to the EDMF parameterization.

The lateral entrainment coefficient has been used for a long time in MF cumulus parameterizations. However, theoretical descriptions of this mixing process are far from being conclusive. Experimental investigations are rare owing to measurement difficulties. Even with the aid of modern computational tools such as LES it is not straightforward to analyze lateral entrainment and formulate physically based ε parameterizations.

In this study we propose a new ε parameterization based on the inverse of the mixing length l:

$$\varepsilon_1 = a_1 \frac{1}{l}, \tag{17}$$

where $a_1 = 0.7$ is a coefficient. Since the mixing length is described mainly in terms of TKE [see Eq. (6), definition of l_1], the new ε formulation is coupled to the TKE closure. This formulation is inspired by a remark in Siebesma et al. (2007) that entrainment is determined by the dominant eddy size at height z, which can be also represented by l. This formulation is also similar to a parameterization based on the inverse of w_u proposed by Neggers et al. (2002, 2009). The square root of TKE can be interpreted as the velocity of the dominant eddies; the more kinetic energy those eddies have, the less time they have to dilute with the environment.

To investigate performance of the new ε formulation we compare results with two other typically used ε parameterizations. The first uses a prescribed profile that depends on the boundary layer height

$$\varepsilon_2 = a_2 \left[\frac{1}{z + \Delta z} + \frac{1}{(z_* - z) + \Delta z} \right], \quad z < z_*, \tag{18}$$

where $a_2 = 0.55$ is a coefficient and Δz (vertical grid spacing) is added to reduce sensitivity to the vertical resolution close to the inversion. This formulation of ε is based on LES results and was previously used in Soares et al. (2004, 2007), Siebesma et al. (2007), and Hurley (2007). One disadvantage of this method is that it is sensitive to the boundary layer height, which is ambiguously defined. As a result, entrainment of dry air from above the inversion can be inaccurate because the entrainment coefficient is fixed with respect to the inversion height. The other reference ε parameterization used here has the form

$$\varepsilon_3 = a_3 \frac{1}{\tau w_u}. \tag{19}$$

In Eq. (19) $a_3 = 2$ is a coefficient, τ [given by Eq. (7)] is a time scale associated with the strongest eddies, and w_u is derived from Eq. (15). This parameterization, but with a constant τ, was proposed by Neggers et al. (2002) and later used by Neggers et al. (2009).

d. Numerical implementation

The integration of the model prognostic Eqs. (2)–(4) is achieved using a semi-implicit Crank–Nicholson scheme. The time discretization follows the scheme originally proposed by Teixeira and Siebesma (2000):

$$\frac{\phi^{t+\Delta t} - \phi^t}{\Delta t} = \frac{\partial}{\partial z}\left(K_\phi^t \frac{\partial \phi^{t+\Delta t}}{\partial z} \right) - \frac{\partial}{\partial z}[M^t(\phi_u^t - \overline{\phi}^{t+\Delta t})] + F_\phi^t. \tag{20}$$

The TKE prognostic equation is discretized in a similar manner with the ED coefficient and the source terms treated explicitly. All equations are solved on a staggered grid with the scalars (ϕ, ϕ_u) being defined on full levels and the variables (e, w_u) on half levels. The first half-level corresponds to the ground. Whenever it is required, a linear interpolation between levels is performed. In space, the prognostic equations are discretized using central differencing, whereas the diagnostic Eqs. (14) and (15) for the updraft properties are discretized using an upstream scheme. This quasi-implicit numerical implementation does not guarantee unconditional stability of the scheme. In fact, some stability issues were observed in simulations with large Courant numbers (e.g., when time steps are

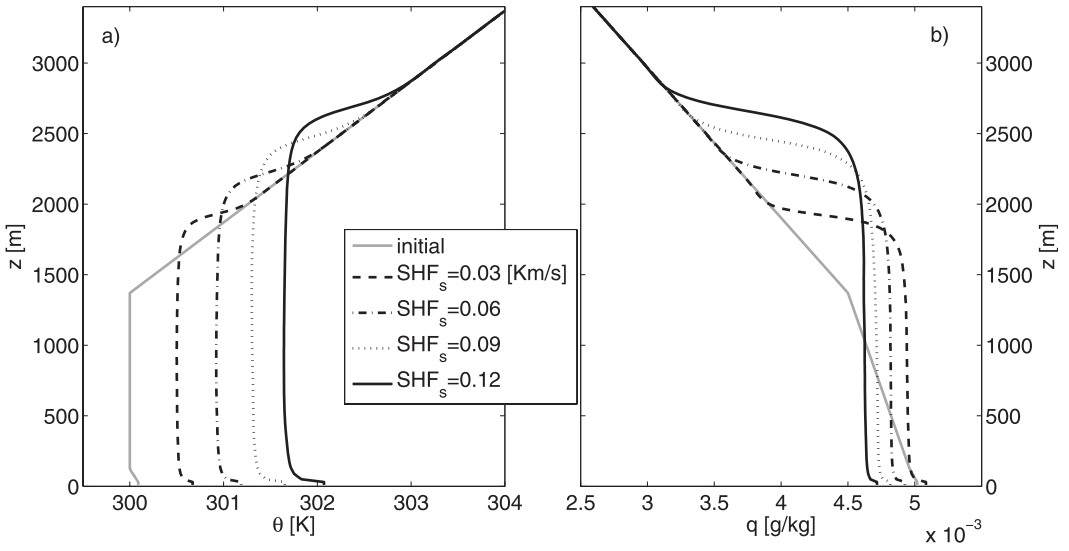

FIG. 2. Vertical profiles of (a) potential temperature and (b) total water mixing ratio at the sixth simulation hour obtained from LES experiments with different SHF_s.

large and vertical resolutions relatively high). This might impose additional numerical constraints when the scheme is implemented in a global or mesoscale model. Nevertheless, numerical stability has been a common and open problem in mesoscale and global models since they often contain such semi-implicit numerical solvers that are not stable under all circumstances.

3. LES experiments

The LES code used in this study is a modified version of the University of California, Los Angeles LES (Stevens et al. 2005; Stevens and Seifert 2008). The Favre-filtered (density weighted) Navier–Stokes equations, written in the anelastic form (Ogura and Phillips 1962; Vallis 2006), are numerically integrated. The constant-coefficient Smagorinsky LES–subgrid-scale (SGS) model (Smagorinsky 1963; Lesieur and Metais 1996) with Lilly's (1962) stability correction is used for turbulent momentum, temperature, and humidity transport. The Smagorinsky coefficient is set to $C_S = 0.23$. Scalar eddy diffusivities are assumed proportional to the momentum eddy diffusivity with a turbulent Prandtl number $\mathrm{Pr}_t = 1/3$. The discrete equations are integrated on a staggered mesh using fully conservative second-order accurate centered differences (Harlow and Welch 1965; Morinishi et al. 1998). Time integration is accomplished by a low-storage third-order Runge–Kutta method (Spalart et al. 1991). The time step is variable and is adjusted to maintain a constant CFL number of 0.3.

A series of four LES runs is performed with various surface sensible heat fluxes (SHF_s) $\overline{w'\theta'_s}$ equal to 0.03, 0.06, 0.09, and 0.12 K m s^{-1}. Initial profiles were based on the profiles established by Nieuwstadt et al. (1992) and further used by Soares et al. (2004), which can be summarized by

$$\theta = 300\,\mathrm{K}, \quad \partial q/\partial z = -3.7\times10^{-4}\ \mathrm{km}^{-1}, \quad 0 < z < 1350\,\mathrm{m},$$
$$\partial\theta/\partial z = 2\,\mathrm{K\,km}^{-1} \quad \partial q/\partial z = -9.4\times10^{-4}\,\mathrm{km}^{-1}, \quad z > 1350\,\mathrm{m}.$$

The initial surface water vapor mixing ratio is 0.005 g g^{-1}. The surface humidity flux is kept constant: $\overline{wq'_s} = 2.5\times10^{-5}$ m s^{-1}. The surface pressure is set to $p_s =$ 1000 hPa. The free convection conditions are assured by setting initial mean wind speed profile as $(u_0, v_0) = (0.01,\ 0)$ m s^{-1}. The LES simulations were performed on a domain with a uniform grid spacing of $\Delta x = \Delta y = \Delta z =$ 20 m. The number of horizontal grid points were 400 × 400, whereas in the vertical 200 and 250 grid points were used for the simulations with surface heat fluxes of (0.03, 0.06) and (0.09, 0.12) K m s^{-1}, respectively. Model results were output every 10 min. Figure 2 shows the initial profiles as well as the LES results from the four simulations at the sixth simulation hour. In all cases three typical regions of the dry convective boundary layer can be identified: (i) the unstable surface layer, stretching from the ground to approximately 100 m, (ii) the well-mixed layer with neutral stratification, and (iii) the capping inversion, also denoted as the entrainment layer, covering the top 10% of the boundary layer. An important test for a 1D model is whether it is able to accurately represent all these characteristic features.

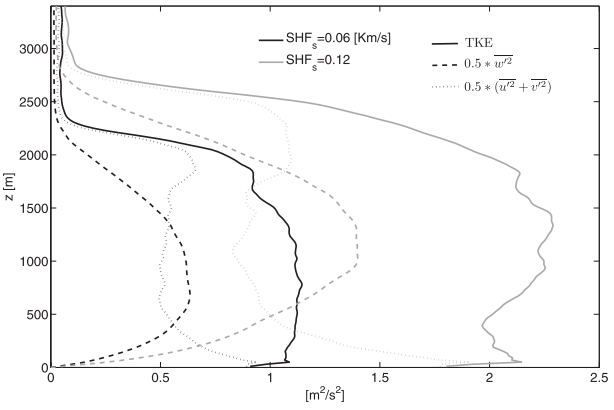

FIG. 3. Vertical structure of TKE and TKE horizontal and vertical components at the sixth simulation hour based on LES runs with $SHF_s = 0.06$ (black lines) and 0.12 (gray lines) (K m s^{-1}): total TKE (solid lines), vertical component of TKE (dashed lines), and the sum of horizontal components of TKE (dotted lines).

Because most parameterizations used in this study are based on TKE, it is valuable to examine the TKE structure simulated by the LES. Figure 3 presents instantaneous vertical profiles of TKE and both vertical and horizontal components of TKE at the sixth hour from simulations with two different surface heat fluxes. In the present discussion, TKE contains only the contribution from the LES-resolved motions because the subgrid TKE is not available from the Smagorinsky model (the isotropic part of the SGS tensor is fused with the dynamic pressure). However, this is an accurate approximation to the total (resolved scale plus subgrid) TKE since the SGS-TKE is only a very small fraction of the total TKE away from the surface (e.g., Schmidt and Schumann 1989). Turbulent kinetic energy (solid lines) is roughly constant with height in most parts of the boundary layer and decreases sharply close to the inversion. The vertical velocity variance profile (dashed lines) has a typical parabolic shape (Schmidt and Schumann 1989; Moeng and Sullivan 1994) with a maximum at around 0.4–0.5 of the boundary layer height (Stull 1988). The constant TKE profile would not be possible without horizontal components of TKE, which dominate in the surface and entrainment layers. They also contribute substantially in the well-mixed layer. In general, horizontal components constitute a large portion of the total TKE even without any large-scale wind forcing.

4. Results

In this section the performance of the 1D model introduced in section 2 is analyzed. The model equations are solved on a 20-m staggered grid with an integration time step set to 60 s. All simulations are initialized with the same conditions as in the LES experiments. Moreover, we performed reference simulations with the ED parameterization in order to assess the relative importance of the MF term versus the ED term. We will proceed by investigating basic CBL characteristics, followed by a more detailed examination of various model features.

a. General profiles and BL height evolution

Figure 4 presents instantaneous profiles of potential temperature (left panel) and total water mixing ratio (right panel) at hour 6 of simulations from LES, EDMF, and ED-only simulations. A clearly good agreement between the EDMF model and the LES results is observed. The surface layer profiles are resolved particularly accurately and the well-mixed layer resembles the LES results closely. The ED simulations, on the other hand, produce slightly unstable profiles in the mid-CBL and a surface layer that is too warm compared to LES. The boundary layer is also higher in the EDMF simulations, following closely the LES results.

To highlight the differences between the models, computations of the boundary layer height z_* and the θ lapse rate in the middle of the well-mixed layer are also shown (Fig. 5). We employ a definition of the inversion height z_* based on the maximum local potential temperature gradient method (Sullivan et al. 1998), following the approach used by Siebesma et al. (2007). For the θ lapse rate computations we consider a layer between 15% and 75% of z_* and fit a linear polynomial to the potential temperature data. Time evolutions of z_* and θ lapse rate from LES, EDMF, and ED simulations are presented in Fig. 5. The results confirm that the EDMF model matches LES well. It preserves the neutrally stratified well-mixed layer at all times and provides the adequate entrainment rate to keep the inversion height close to the LES values. Initial disagreement between models (first 100 min) is due to a spinup effect.

The EDMF model results, however, are not in a perfect match to LES. Some differences are apparent in the inversion layer structure (Fig. 4) and in slight deviations in the inversion height (Fig. 5a), especially for the strong surface heating scenarios. Also, the entire boundary layer gets a slight negative temperature bias as the surface heat flux increases. Furthermore, there are disagreements in the humidity profiles: q is somewhat underestimated and not sufficiently well mixed in the CBL. These indicate that the 1D model has still some difficulties in producing a precise representation of CBL mixing and top entrainment. We investigate in detail other characteristics of the model in order to understand these deficiencies.

b. Updraft characteristics

We start by examining the MF component, a crucial term in the new model. Figure 6 presents the difference

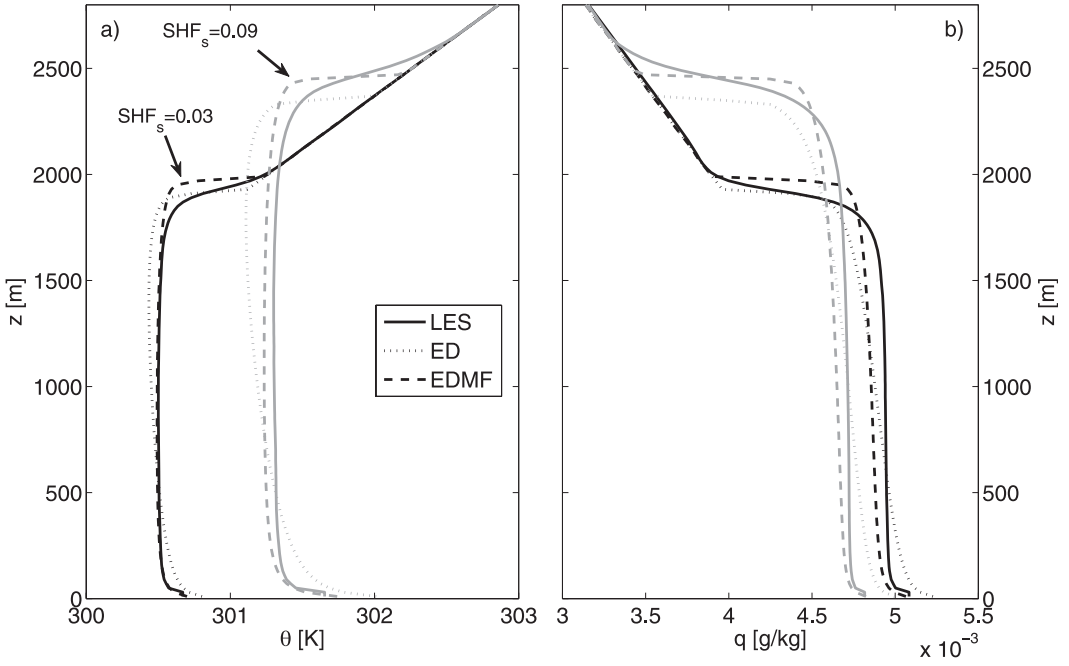

FIG. 4. Vertical profiles of (a) θ and (b) q obtained with the LES, EDMF, and ED-only simulations: $\mathrm{SHF}_s = 0.03$ K m s^{-1} (black lines) and 0.09 K m s^{-1} (gray lines).

between the updraft temperature and the environment (left panel) and the updraft vertical velocity (right panel) derived from the 1D model and LES simulations. Results are averaged ±30 min around the sixth hour of the LES runs. The LES updraft values are obtained by averaging over the 10% largest values of the vertical velocity distribution at each model level. There is fairly good agreement in the updraft temperature excess (Fig. 6a) as well as in w_u (Fig. 6b) between the EDMF and LES models. In particular, the 1D model is quite accurate in resolving the updraft velocity and general structure of the updraft temperature excess. However, the temperature excess is mostly overestimated in the EDMF, especially in the middle of the boundary layer. Moreover, the discrepancies seem to depend on surface fluxes, which becomes evident when the temperature excess structure at the inversion is compared. Some disagreements are also found in the surface layer.

The 1D model underestimates the updraft temperature excess in the surface layer. This is directly related to the initialization method, given by Eq. (16). We set β to 0.3, which is a value established in previous studies (Soares et al. 2004). However, when this coefficient is increased to a much larger value, for instance 2.5, a much better agreement with the LES results in the surface layer is obtained (results not shown here). Moreover, setting β to 2.5 does not impair good agreement in the middle of the CBL and has a negligible effect on the inversion structure. These findings are similar to the results obtained by Siebesma et al. (2007), who also noticed low sensitivity of the boundary layer height evolution on the updraft initialization procedure. Given that β has a limited influence on the upper parts of the boundary layer, the previously established value 0.3 is retained. We leave possible changes to future research.

More important, from the model performance point of view, are the differences in the inversion layer. The 1D model underestimates updraft overshooting, especially in the simulations with higher surface heat fluxes. The vertical velocity inside updrafts (Fig. 6b) quickly goes to zero at the top of CBL and the updrafts are not able to penetrate deeper into the inversion. This results in a lower entrainment rate and steepening of average profiles at the top of CBL (see also Fig. 4). The rapid slowdown of w_u is mostly related to the sharp lateral entrainment increase at the inversion, Eq. (15). In this study we use a formulation where the entrainment coefficient ε is an inverse function of the mixing length, and de facto of the TKE [Eq. (17)]. Investigating the TKE structure from the 1D and LES models might provide an insight into the sources of disagreement between the models.

c. TKE structure

In Fig. 7a the normalized and averaged TKE profiles derived from the LES and 1D models are compared. There is general agreement between the TKE profiles,

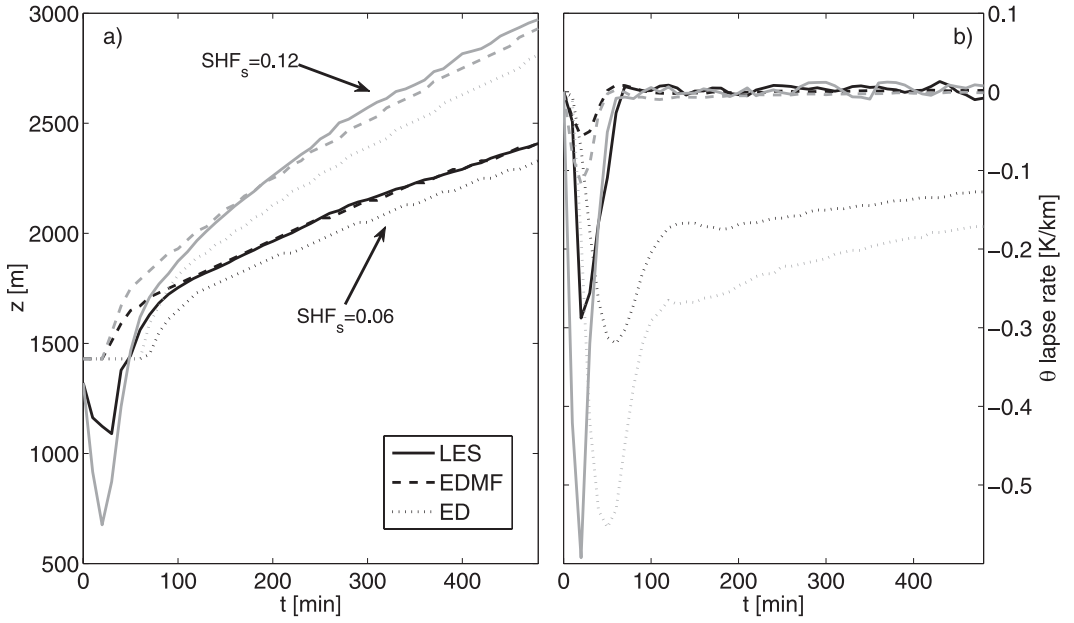

FIG. 5. Temporal evolution of the (a) BL height and (b) θ lapse rate as obtained from the LES, EDMF, and ED-only simulations: SHF$_s$ = 0.06 K m s^{-1} (black lines) and 0.12 K m s^{-1} (gray lines).

but the 1D model is clearly missing some important features. It cannot reproduce the fairly constant TKE values throughout the boundary layer found in LES and underestimates turbulence in the upper parts of the CBL. This last shortcoming is especially relevant for the representation of top entrainment, making it too weak compared to LES (Fig. 6a).

Possible reasons behind the TKE differences are investigated in Fig. 7b. Black and gray lines represent budget terms of TKE from LES and EDMF, respectively. Only the normalized buoyancy source term $\overline{w'\theta'_v}g/\overline{\theta}_v$ (solid lines) and the transport term (dashed lines) are presented. The transport term is given by $\partial(K_e\partial e/\partial z)/\partial z$ in the 1D model, whereas in the LES is calculated according to

$$\text{trans} = -\frac{\partial\overline{w'e'}}{\partial z} - \frac{\partial\overline{w'p'}}{\partial z}, \tag{21}$$

where p' stands for the pressure fluctuations. Assuming that TKE dissipation scales only with TKE itself, the

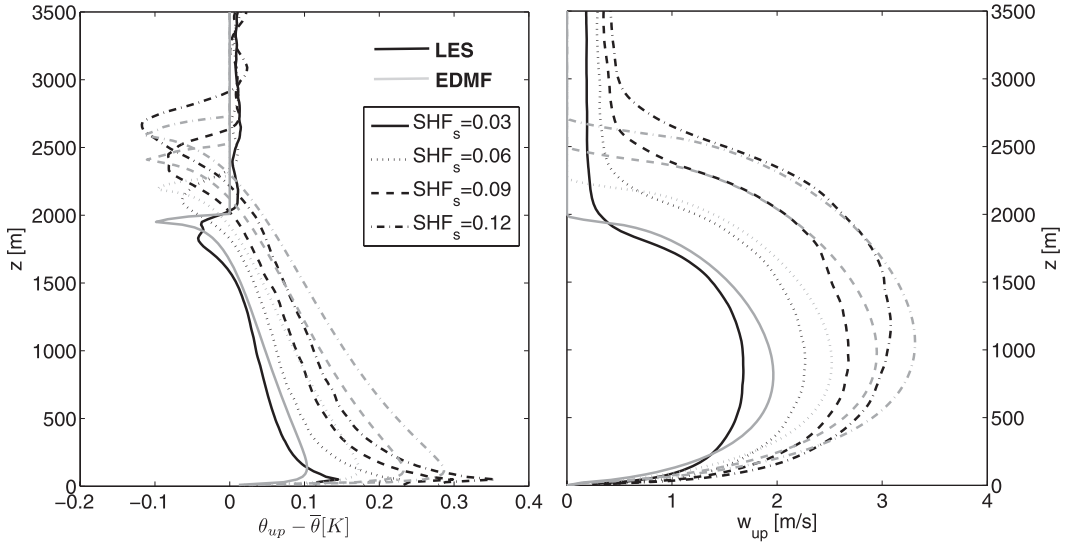

FIG. 6. Updraft characteristics obtained from the LES and EDMF simulations with different SHF$_s$: (a) updraft θ excess and (b) updraft vertical velocity. Results are averaged over the sixth simulation hour (6 h ± 30 min).

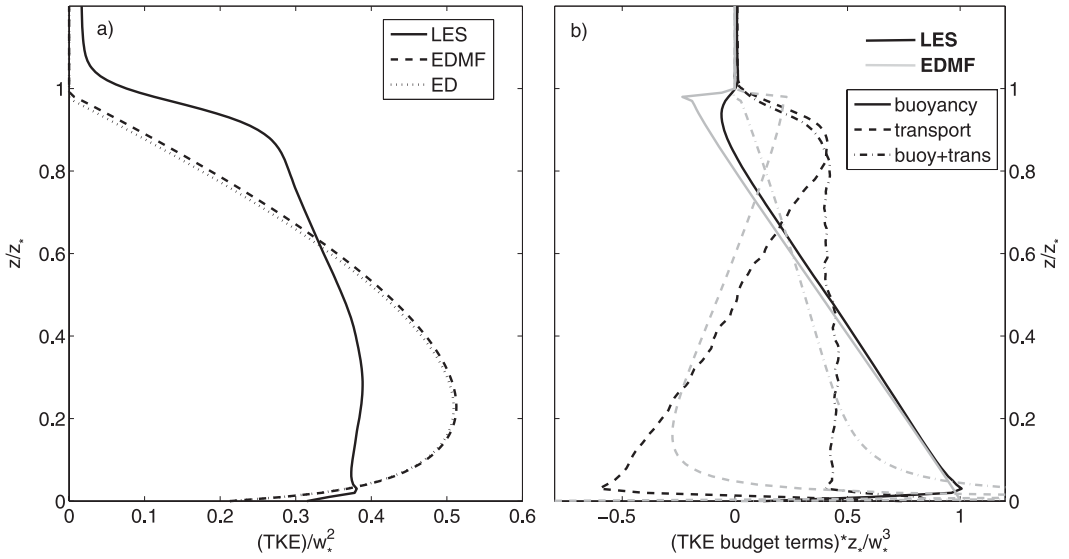

FIG. 7. (a) Normalized and averaged TKE profiles from the LES, EDMF, and ED-only simulations. (b) Normalized and averaged TKE budget components from the LES (black) and EDMF (gray) simulations.

profile of this sum should determine the profile of TKE. This seems to be the case in the LES simulations, where the two budget terms add up to a profile that is roughly constant with height (black dotted–dashed line). In the 1D model the sum of both budget terms (gray dotted–dashed line) has a steep increase close to the surface and in the middle of CBL decreases linearly with height. The similar pattern is only partially observed in the TKE profile obtained from the 1D model. That is because of the lower boundary conditions imposed in the TKE prognostic equation; see Eq. (13). Those conditions limit the growth of TKE close to the surface and are responsible for the parabolic-like shape of the TKE profile in the 1D model simulations.

Another apparent difference in the budget terms of TKE that can be seen in Fig. 7b is in the transport terms. The transport mechanisms are much less efficient in the 1D simulations, leading to substantial underestimation of TKE at the inversion. This could be due to K_e being too small or having an improper vertical profile. To investigate if this is the case a number of sensitivity studies were performed. These involved increasing K_e and modifying its profile in an attempt to get much closer correspondence of the 1D and LES transport terms. Results (not shown) suggest that, although by changing K_e a better agreement close to the surface can be obtained, the 1D transport always remains underestimated in the upper parts of the CBL and close to the inversion. Furthermore, by modifying K_e to improve this one aspect of the LES–EDMF comparison the overall accuracy of the simulations is substantially reduced. These results suggest that the ED parameterization is not sufficiently accurate to represent the TKE transport in the dry CBL. It was already mentioned by Schumann and Moeng (1991b) that updrafts themselves, through transport and lateral mixing, are important sources of TKE in the upper parts of the CBL. Updrafts that reach the inversion lose their vertical momentum and change direction, thus creating dynamical instabilities. This mechanism is expected to contribute to the TKE near the inversion. It can be also argued that updrafts could transport TKE in the same manner as they transport scalar variables. Such an idea, however, faces several conceptual difficulties. It is not clear at this stage how to calculate e_u and how it should be initialized. One possible approach, adopted by Angevine et al. (2010), is to treat TKE as a scalar and initialize it in a manner similar to θ_u. Moreover, updrafts themselves are part of TKE and in order to include the MF transport one should model separately a small-scale and a large-scale TKE. Such splitting poses further uncertainties and difficulties. Regardless of these problems it seems justified that some other TKE transport mechanisms are necessary to properly simulate TKE in the CBL. The ideas proposed above, or some other concepts, should be further investigated to address this topic.

d. Resolution and time step sensitivity

Potential implementations of the EDMF approach proposed here in weather and climate models would require different vertical and temporal resolutions than those used in the present simulations. Twenty-meter resolution is often used close to the surface in large-scale

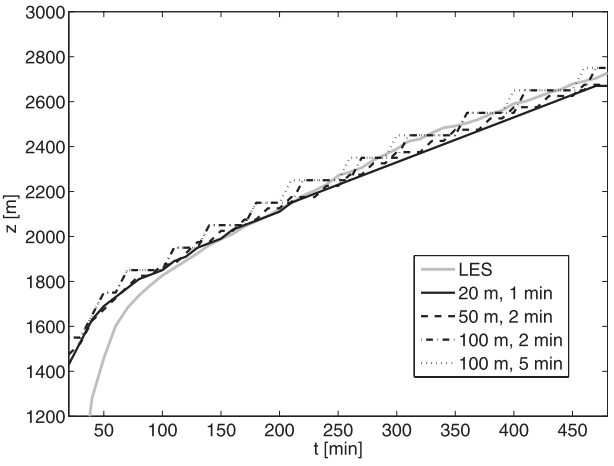

FIG. 8. Boundary layer height evolution from LES and EDMF simulations with different vertical and temporal resolutions; simulations performed with $\mathrm{SHF}_s = 0.09$ K m s^{-1}.

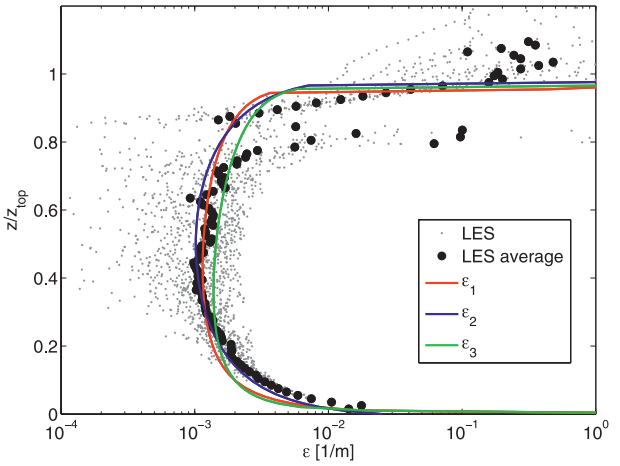

FIG. 9. Entrainment coefficient diagnosed from LES and obtained from three different ε parameterizations.

models, but higher in the BL, or in the free troposphere grid resolution typically degrades, easily exceeding 100 m. Also, the integration time step in forecast models is set to different values, often depending on the vertical resolution and stability constraints related to the Courant number. To test the sensitivity of the new 1D model, the impact of decreased vertical and temporal resolutions on the evolution of the boundary layer height is investigated. Figure 8 presents results of the simulations with surface heat flux 0.09 K m s^{-1} for various resolution setups. For the range of investigated cases (20–100 m, 1–5 min) the 1D model proves very robust in terms of its sensitivity to resolution. The CBL height dynamics is captured well in all situations. Further increase of the time step at 100-m grid spacing leads to stability issues. For even coarser vertical resolution (over 200 m) results diverge from LES, with a tendency to overestimate the CBL height. These issues require further study.

5. Entrainment coefficient comparison

A crucial parameter of the EDMF parameterization is ε. In this study a new formulation based on an inverse of the mixing length, and de facto of the TKE, is used. Two other approaches have been previously employed by investigators, as described in section 2. One uses a prescribed profile based on the boundary layer height and the other is based on the inverse of the updraft velocity. In this section we compare these different formulations and assess their usefulness in 1D simulations. We also use LES-derived lateral entrainment values to validate ε parameterizations.

The lateral entrainment coefficient can be diagnosed from LES results using Eq. (14). Results are typically noisy, and below the inversion there is additional difficulty when $\theta_u - \overline{\theta}$ crosses zero and the solution becomes ill defined. Given that sufficiently large statistics is provided, an averaging procedure can be applied to get a consistent ε profile. We use four LES simulations with different surface heat fluxes, but at a time when all have the same CBL height. We chose $z_* = 1900 \pm 50$ m, which gives a sample of 22 ε profiles diagnosed from LES. Figure 9 presents individual ε results (gray dots) along with averaged values (black circles). Lateral entrainment profiles obtained with different ε parameterizations are presented in solid lines.

There is good agreement between the diagnosed and simulated lateral entrainment profiles (Fig. 9), given the spread of LES values. Lateral entrainment values in the well-mixed layer are $O(10^{-3})$, a value often assumed in cumulus clouds, diagnosed from other LES studies (e.g., Siebesma and Cuijpers 1995) and consistent with a CBL depth $O(10^3)$ m. Different ε parameterizations give quite similar results, despite distinct formulations. This justifies the use of different approaches by previous investigators and gives confidence in the TKE-based parameterization proposed in this study. All parameterizations seem to create too sharp of an increase of ε at the top of the boundary layer, compared to LES. This influences updraft evolution and impacts boundary-layer-top entrainment of air from the free troposphere into the CBL.

Figure 10a shows that all three ε parameterizations produce almost exactly the same θ profiles. Evolution of the boundary layer height and the θ lapse rate in the well-mixed layer are also analogous. However, there are some structural differences that become apparent when other model parameters are examined. These differences influence parameterization consistency and prospects for further development. First, the robustness of

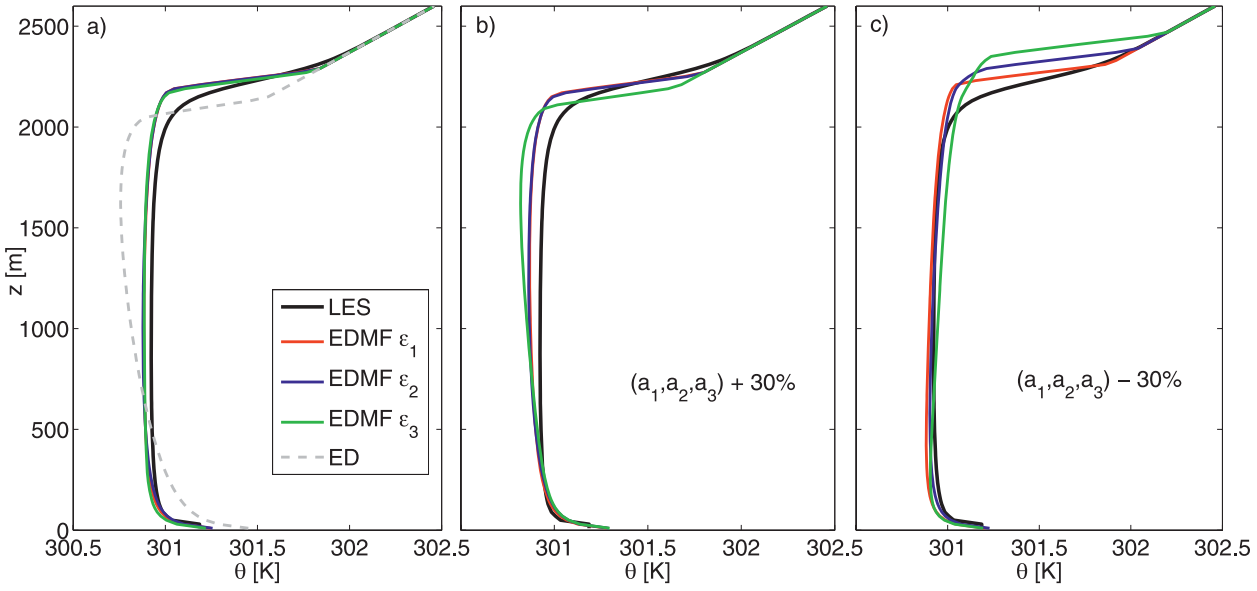

FIG. 10. (a) Average θ profiles (6 h $\pm$ 30 min) as simulated with LES and EDMF model with three different ε parameterizations; (b),(c) as in (a) but after scaling ε by (b) +30% and (c) −30%.

each parameterization by performing a sensitivity study of the formulations to the used parameters is examined. In each case the parameters a_1, a_2, and a_3 from Eqs. (17), (18), and (19) are modified by $\pm$30%. Results are presented in Figs. 10b and 10c. By increasing the parameters by 30% the lateral entrainment is increased and thus the mass flux component is reduced. This results in lower CBL heights and slightly unstable θ profiles in the middle of the CBL. Simulations with ε_1 and ε_2 produce the same results, whereas ε_3 is clearly worse than the other two with lower boundary layer height and greater instability in the well-mixed layer. A decrease in the parameters by 30% (Fig. 10c) results in stronger updrafts that can more vigorously penetrate the inversion. The CBL top is higher and the simulated profiles become excessively stable due to entrainment of warmer air from above the inversion. The ε_1 parameterization agrees best with LES results in this case. In general, the TKE-based lateral entrainment parameterization proves to be the most robust with respect to its sensitivity to changes in the parameter space.

There is an additional feature of the parameterizations ε_2 and ε_3 that makes these schemes less consistent with a CBL closure based on TKE. In the case of a decrease in a_2 and a_3 parameters, a region forms at the inversion where there are still penetrating updrafts (nonzero w_u) but the TKE is already zero. Such behavior seems to be not physically justified and is in contradiction to LES results. In numerical realization this decoupling of the MF transport and TKE often results in ''wiggles'' in the θ and q profiles at the interface. This is because there is no local ED transport that would assure smooth behavior. In Fig. 10 the results are smoothed out by averaging over 1 h. This decoupling could be possibly tackled by introducing a MF transport of TKE. A short discussion on this issue has been presented in a previous section.

The lateral entrainment parameterization affects updraft characteristics. It is therefore useful to examine the updraft properties simulated with the three different ε formulations. Figure 11 shows $(\theta_u - \overline{\theta})/\theta_*$ (left panel, $\theta_* = \overline{w'\theta_v'}^s/w_*$) and w_u/w_* (right panel), normalized and averaged over last 6 h of the simulations. Simulations with the three ε parameterizations (a_1, a_2, and a_3 are not modified) along with LES results are presented. All parameterizations produce comparable updraft characteristics, being in general agreement with the LES results. Most important differences occur at the inversion in the θ_u structure and in the middle of the boundary layer in the w_u profile. All parameterizations produce an inversion that is too shallow in its vertical extent, compared to LES. The prescribed ε_2 parameterization produces too strong θ_u overshooting, whereas ε_3 has slightly underestimated $\theta_u - \overline{\theta}$ values at the inversion. The w_u values from all ε parameterizations are overestimated by less than 20% in the middle of the boundary layer, with the maxima varying with height among various formulations. Updraft velocities are in good agreement with LES in the surface layer and below the inversion, but decrease sharply at $z/z_* \rightarrow 1$. In general, the ε_1 parameterization produces the most reasonable θ_u and w_u profiles when compared to LES.

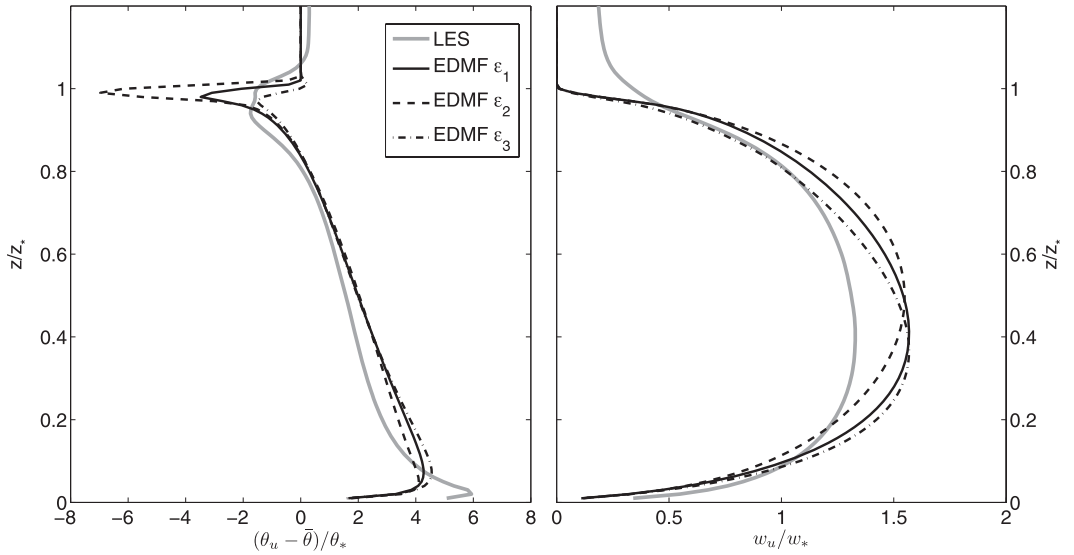

FIG. 11. Normalized and averaged updraft characteristics as simulated with LES and EDMF model with three different ε parameterizations: (a) updraft θ excess and (b) updraft vertical velocity.

Results presented above indicate that the lateral entrainment parameterization based on TKE provides results similar to the results obtained with the use of two other previously established parameterizations. Moreover, the new parameterization proves more robust to changes of the coefficients used and also gives better characteristics of the updraft properties compared to the LES results.

6. Summary and conclusions

Modeling of dry convective boundary layers remains a significant challenge in weather and climate projection simulations. The realistic representation of subgrid-scale processes such as turbulent countergradient fluxes or the boundary-layer-top entrainment have for long been a major problem in the modeling community. The recent emergence of the EDMF framework, backed by LES simulations, improves our understanding of convective processes and our ability to parameterize different scales of the transport mechanisms. EDMF has proved to be a useful approach not only in the dry convection case, but also as a potential candidate to unify all boundary layer parameterizations in a single method.

In this study we extend the concept of EDMF to a scheme that is coupled with a TKE prognostic equation. Such coupling exerts feedback mechanisms between TKE and MF through the buoyancy source term and the lateral entrainment coefficient. This leads to a closer relation between the updraft velocity and TKE, and an increased robustness compared to other approaches. The proposed scheme is a significant step toward merging EDMF with higher-order closures and taking direct advantage of the capabilities of using TKE in weather and climate forecasting.

In section 2 we introduce the governing prognostic equations and the parameterizations used to close these equations. Important parts include the mixing length formulation, surface layer scaling, and lateral entrainment parameterization. The Monin and Obukhov (1954) free-convection similarity scaling is essential to realistically resolve the profiles close to the surface. It is also used to provide boundary conditions for the TKE prognostic equation. The lateral entrainment coefficient ε influences updraft characteristics and is responsible for the exchange of properties between the updrafts and environment. Along with the new ε parameterization we describe two other ε formulations that have been previously used by investigators. All three approaches are further compared in section 5.

The EDMF framework embedded in a 1D model is evaluated against LES simulations. Several dry convection cases with different surface heat fluxes are used. As an initial condition we use the Nieuwstadt et al. (1992) and Soares et al. (2004) profiles of potential temperature and total water mixing ratio. In section 4 we present results of 1D and LES simulations and evaluate different model characteristics. The new scheme is very accurate in representing the structure and evolution of the mean model variables. It is able to properly capture the CBL height dynamics and the well-mixed neutral profile in the middle of the CBL. Moreover, the new 1D model is quite robust in respect to its sensitivity to vertical and temporal resolution changes. The updraft characteristics are

in good agreement with LES. Some disagreements are observed in the surface layer and at the inversion. Those have been found to depend on the updraft initialization procedure and the TKE discrepancies between the 1D and LES models. The analysis of the TKE budget terms in the 1D model revealed underestimation of the TKE transport from close to the surface to the upper parts of CBL. This prevents the simulated TKE to have a roughly constant value in a CBL and leads to disagreements with the profiles derived from LES. It is possible that including mass-flux transport of TKE would improve the 1D predictions and overall performance of the EDMF parameterization. In their recent study, Angevine et al. (2010) introduce such a MF term for vertical transport of the total turbulent energy, although they do not elaborate on the specifics of their formulation. They conclude that their parameterization gives more realistic profiles for shallow cumulus conditions than more traditional boundary layer schemes. However, it remains uncertain how the MF transport of total turbulence contributes to the performance of their scheme. This topic should be investigated in further research.

Finally, different lateral entrainment parameterizations are compared in section 5. To our knowledge it is the first attempt to compare and evaluate various formulations of this important parameter of the EDMF framework. The parameterizations produce similar ε profiles that match the LES diagnosed values relatively well. Some differences are still evident and have consequences in simulated updraft characteristics. The parameterization based on the vertical velocity underestimates updraft overshooting at the inversion. The parameterization based on the prescribed profile, on the other hand, substantially overestimates θ_u excess at the inversion. The new parameterization based on TKE produces updraft characteristics that are in best agreement with the LES results. Sensitivity study results show that increasing or decreasing ε by 30% also favors the new parameterization over other approaches. The TKE-based parameterization proves the most robust with respect to changes in the scaling coefficient. Additionally, it does not allow for an unphysical decoupling of updrafts and TKE at the top of CBL. The previous ε parameterizations permit updrafts to penetrate inside the inversion where the simulated TKE is close to zero. This creates an inconsistency since updrafts are obviously a part of turbulent motions. The new ε parameterization does not suffer from this deficiency.

Acknowledgments. We thank Bjorn Stevens for providing and assisting us with the UCLA-LES code. We would also like to thank the Center for Advanced Computing Research at Caltech for technical assistance. This research was carried out at the Jet Propulsion Laboratory, California Institute of Technology, under a contract with the National Aeronautics and Space Administration. The authors acknowledge the support provided by the Office of Naval Research, Marine Meteorology Program under award N0001408IP20064 and the NASA MAP Program.

REFERENCES

Abdella, K., and N. A. McFarlane, 1996: Parameterization of the surface-layer exchange coefficients for atmospheric models. *Bound.-Layer Meteor.,* **80,** 223–248.

Angevine, W. M., 2005: An integrated turbulence scheme for the boundary layer with shallow cumulus applied to pollutant transport. *J. Appl. Meteor.,* **44,** 1436–1452.

——, H. Jiang, and T. Mauritsen, 2010: Performance of an eddy diffusivity–mass flux scheme for shallow cumulus boundary layers. *Mon. Wea. Rev.,* **138,** 2895–2912.

Arakawa, A., and W. H. Schubert, 1974: Interaction of a cumulus cloud ensemble with the large-scale environment, Part I. *J. Atmos. Sci.,* **31,** 674–701.

Beljaars, A. C. M., 1995: The parameterization of surface fluxes in large-scale models under free convection. *Quart. J. Roy. Meteor. Soc.,* **121,** 255–270.

Betts, A. K., 1973: Non-precipitating cumulus convection and its parameterization. *Quart. J. Roy. Meteor. Soc.,* **99,** 178–196.

Blackadar, A., 1962: The vertical distribution of wind and turbulent exchange in a neutral atmosphere. *J. Geophys. Res.,* **67,** 3095–3102.

Cheinet, S., 2003: A multiple mass-flux parameterization for the surface-generated convection. Part I: Dry plumes. *J. Atmos. Sci.,* **60,** 2313–2327.

——, and J. Teixeira, 2003: A simple formulation for the eddy-diffusivity parameterization of cloud-topped boundary layers. *Geophys. Res. Lett.,* **30,** 1930, doi:10.1029/2003GL017377.

Deardorff, J. W., 1966: The counter-gradient heat flux in the lower atmosphere and in the laboratory. *J. Atmos. Sci.,* **23,** 503–506.

Harlow, F. H., and J. E. Welch, 1965: Numerical calculation of time-dependent viscous incompressible flow of fluid with free surface. *Phys. Fluids,* **8,** 2182–2189.

Holtslag, A. A. M., and C.-H. Moeng, 1991: Eddy diffusivity and countergradient transport in the convective atmospheric boundary layer. *J. Atmos. Sci.,* **48,** 1690–1698.

Hurley, P., 2007: Modeling mean and turbulence fields in the dry convective boundary layer with the eddy-diffusivity/mass-flux approach. *Bound.-Layer Meteor.,* **125,** 525–536.

Lappen, C.-L., and D. A. Randall, 2001: Toward a unified parameterization of the boundary layer and moist convection. Part I: A new type of mass-flux model. *J. Atmos. Sci.,* **58,** 2021–2036.

Lesieur, M., and O. Metais, 1996: New trends in large-eddy simulations of turbulence. *Annu. Rev. Fluid Mech.,* **28,** 45–82.

Lilly, D. K., 1962: On the numerical simulation of buoyant convection. *Tellus,* **14,** 148–172.

Moeng, C. H., and P. Sullivan, 1994: A comparison of shear- and buoyancy-driven planetary boundary layer flows. *J. Atmos. Sci.,* **51,** 999–1022.

Monin, A. S., and A. M. Obukhov, 1954: Basic regularity in turbulent mixing in the surface layer of the atmosphere. *Akad. Nauk. S.S.S.R. Trud. Geofiz. Inst.,* **24,** 163–187.

Morinishi, Y., T. S. Lund, O. V. Vasilyev, and P. Moin, 1998: Fully conservative higher order finite difference schemes for incompressible flow. *J. Comput. Phys.,* **143,** 90–124.

Nakanishi, M., 2001: Improvement of the Mellor–Yamada turbulence closure model based on large-eddy simulation data. *Bound.-Layer Meteor.,* **99,** 349–378.

Neggers, R. A. J., 2009: A dual mass flux framework for boundary layer convection. Part II: Clouds. *J. Atmos. Sci.,* **66,** 1489–1506.

——, A. P. Siebesma, and H. J. J. Jonker, 2002: A multi-parcel model for shallow cumulus convection. *J. Atmos. Sci.,* **59,** 1655–1668.

——, M. Köhler, and A. C. M. Beljaars, 2009: A dual mass flux framework for boundary layer convection. Part I: Transport. *J. Atmos. Sci.,* **66,** 1465–1487.

Nieuwstadt, F. T. M., P. J. Mason, C.-H. Moeng, and U. Schumann, 1992: Large-eddy simulation of the convective boundary layer: A comparison of four codes. *Turbulent Shear Flows 8: Selected papers from the Eighth International Symposium on Turbulent Shear Flows,* F. Durst et al., Eds., Springer, 343–367.

Ogura, Y., and N. A. Phillips, 1962: Scale analysis of deep and shallow convection in the atmosphere. *J. Atmos. Sci.,* **19,** 173–179.

Ooyama, K., 1971: A theory on parameterization of shallow cumulus convection. *J. Meteor. Soc. Japan,* **49,** 744–756.

Paulson, C. A., 1970: The mathematical representation of wind speed and temperature profiles in the unstable atmospheric surface layer. *J. Appl. Meteor.,* **9,** 857–861.

Potty, K. V. J., U. C. Mohanty, and S. Raman, 2001: Simulation of boundary layer structure over the Indian summer monsoon trough during the passage of a depression. *J. Appl. Meteor.,* **40,** 1241–1254.

Randall, D. A., Q. Shao, and C.-H. Moeng, 1992: A second-order bulk boundary-layer model. *J. Atmos. Sci.,* **49,** 1903–1923.

Schmidt, H., and U. Schumann, 1989: Coherent structure of the convective boundary layer derived from large-eddy simulations. *J. Fluid Mech.,* **200,** 511–562.

Schumann, U., and C.-H. Moeng, 1991a: Plume fluxes in clear and cloudy convective boundary layers. *J. Atmos. Sci.,* **48,** 1746–1757.

——, and ——, 1991b: Plume budgets in clear and cloudy convective boundary layers. *J. Atmos. Sci.,* **48,** 1758–1770.

Siebesma, A. P., and J. W. M. Cuijpers, 1995: Evaluation of parametric assumptions for shallow cumulus convection. *J. Atmos. Sci.,* **52,** 650–666.

——, and J. Teixeira, 2000: An advection–diffusion scheme for the convective boundary layer: Description and 1D results. *Proc. 14th Symp. on Boundary Layers and Turbulence,* Aspen, CO, Amer. Meteor. Soc., 133–136.

——, P. M. M. Soares, and J. Teixeira, 2007: A combined eddy-diffusivity mass-flux approach for the convective boundary layer. *J. Atmos. Sci.,* **64,** 1230–1248.

Simpson, J., and V. Wiggert, 1969: Models of precipitating cumulus towers. *Mon. Wea. Rev.,* **97,** 471–489.

Smagorinsky, J., 1963: General circulation experiments with the primitive equations. I. The basic experiment. *Mon. Wea. Rev.,* **91,** 99–164.

Soares, P. M. M., P. M. A. Miranda, A. P. Siebesma, and J. Teixeira, 2004: An eddy-diffusivity/mass-flux parameterization for dry and shallow cumulus convection. *Quart. J. Roy. Meteor. Soc.,* **130,** 3365–3383.

——, ——, J. Teixeira, and A. P. Siebesma, 2007: An eddy-diffusivity/mass-flux boundary layer parameterization based on the turbulent kinetic energy equation. *Fis. Tierra,* **19,** 147–161.

Spalart, P. R., R. D. Moser, and M. M. Rogers, 1991: Spectral methods for the Navier–Stokes equations with one infinite and two periodic directions. *J. Comput. Phys.,* **96,** 297–324.

Stevens, B., 2000: Quasi-steady analysis of a PBL model with an eddy-diffusivity profile and nonlocal fluxes. *Mon. Wea. Rev.,* **128,** 824–836.

——, and A. Seifert, 2008: Understanding macrophysical outcomes of microphysical choices in simulations of shallow cumulus convection. *J. Meteor. Soc. Japan,* **86A,** 143–162.

——, and Coauthors, 2005: Evaluation of large-eddy simulations via observations of nocturnal marine stratocumulus. *Mon. Wea. Rev.,* **133,** 1443–1462.

Stull, R. B., 1988: *An Introduction to Boundary Layer Meteorology*. Kluwer Academic, 666 pp.

Sullivan, P. P., C. H. Moeng, B. Stevens, D. H. Lenschow, and S. D. Mayor, 1998: Structure of the entrainment zone capping the convective atmospheric boundary layer. *J. Atmos. Sci.,* **55,** 3042–3064.

Suselj, K., and A. Sood, 2010: Improving Mellor–Yamada–Janjic parameterization for the wind conditions in the marine planetary boundary layer. *Bound.-Layer Meteor.,* **136,** 301–324.

Teixeira, J., and A. P. Siebesma, 2000: A mass-flux/*K*-diffusion approach to the parameterization of the convective boundary layer: Global model results. *Proc. 14th Symp. on Boundary Layers and Turbulence,* Aspen, CO, Amer. Meteor. Soc., 231–234.

——, and S. Cheinet, 2004: A simple mixing length formulation for the eddy-diffusivity parameterization of dry convection. *Bound.-Layer Meteor.,* **110,** 435–453.

——, J. P. Ferreira, P. M. A. Miranda, T. Haack, J. Doyle, A. P. Siebesma, and R. Salgado, 2004: A new mixing-length formulation for the parameterization of dry convection: Implementation and evaluation in a mesoscale model. *Mon. Wea. Rev.,* **132,** 2698–2707.

Vallis, G. K., 2006: *Atmospheric and Oceanic Fluid Dynamics: Fundamentals and Large-Scale Circulation*. Cambridge University Press, 745 pp.

Wang, S., and B. A. Albrecht, 1990: A mean-gradient model of the dry convective boundary layer. *J. Atmos. Sci.,* **47,** 126–138.

Wyngaard, J. C., 1992: Atmospheric turbulence. *Annu. Rev. Fluid Mech.,* **24,** 205–233.